Undoing of firing rate adaptation enables invariant population codes

Brandão S.C. [1†], Ramirez L. [1†], Walter A.M. [2], Silies M. [1], Martelli C. [1‡]

[1]Institute of Developmental Biology and Neurobiology, Johannes Gutenberg University, Mainz, Germany
[2]University of Copenhagen, Denmark
[†] These authors contributed equally to this work.

[‡] Corresponding author: cmartell@uni-mainz.de

Summary

Adaptation often implements an efficient coding strategy to align neuron sensitivity to relevant stimuli. However, when sensory information is encoded in populations of neurons, adaptation of individual units could deteriorate stimulus information relevant for behavior. One prominent example is the encoding of olfactory information, which occurs at the population level. We show that if individual ORNs were to adapt following an efficient coding principle, contrast information would be lost at the population level, impairing the detection of ON and OFF stimuli. Surprisingly, adaptation of ORN firing responses is compensated at the axon terminal, where calcium transients are kept background-invariant by inhibitory feedback. We demonstrate that achieving this invariance across different background conditions requires an adaptation strategy that shifts response amplitude, rather than sensitivity as predicted by the efficient coding principle. This background invariance is passed on to second-order olfactory neurons, through facilitation of vesicle release that involves modulation of Unc13 proteins. We conclude that synaptic and circuit computations compensate peripheral firing rate adaptation, enhancing the separation of ON and OFF contrasts, while preserving the identity of ON stimuli in population codes. Our findings identify a strategy that allows neural circuits to minimize the cost of information transmission while preserving information content.

Introduction

Neural adaptation is an essential strategy of sensory systems that allows the encoding of stimuli over a range of intensities exceeding the limits of the individual sensory cell[1]. To achieve this plasticity, neurons tune their stimulus-response function to the relevant statistics of the stimulus[2]. For instance, efficient coding theories at the single-neuron level predict that a shift in neuron sensitivity that matches the mean of the stimulus optimizes the encoding of relevant information within the neuron dynamic range[3]. Such shifts in sensitivity have been observed in several sensory systems, from audition to vision, in artificial and natural conditions[4,5]. However, very little is known about the role of adaptation in olfaction. The olfactory system is by design endorsed with a large array of sensory receptors with different affinities to the same odorant[6,7]. When the stimulus intensity (concentration) increases, the more sensitive receptors saturate while new ones with lower affinity are recruited. Therefore, the system as a whole is rarely out of its broad dynamic range. While the benefits of adaptation in single neurons have been widely discussed[8,9], the benefits of single neuron adaptation at the population level require a deeper understanding. Studies in the visual cortex suggest that neuronal adaptation can improve coding accuracy at the population level in a stimulus dependent manner[10] . However, the function and potential benefits of adaptation in populations of olfactory neurons remain largely unexplored.

In both vertebrates and invertebrates, the firing rate of Olfactory Receptor Neurons (ORNs) decreases upon persistent stimulation[11–17], inducing a change in their response curve. Yet, the coding function of this adaptive change remains poorly understood. On one hand, a decreased in ORN response could lead to a decrease in perception of the odor stimulus. However the relationship between ORN adaptation and decreased stimulus perception is so far correlative[18] since a decreased behavioural response to persistent odour stimuli could derive from plasticity (e.g. habituation[19–21]) in higher brain areas rather than from decreased receptor sensitivity. On the other hand, adaptation of the sensory neurons could play a role

in odor-driven navigation. Behavioral studies in *Drosophila* suggest that flies can implement a chemotactic strategy for odor-guided searching behaviour[22,23]. In single cell organisms, such as bacteria, chemotaxis relies on receptor adaptation for contrast computations[24]. Such contrast computations could in principle also occur in the ORNs[25,26], although the contrast sensitivity of these neurons across a physiological range of concentrations remains debated[27,28]. Importantly a contrast computation in single ORNs prior to the encoding of odor identity across the ORN population could interfere with information transmission in downstream circuits. Ultimately, to understand the role of peripheral ORN adaptation is necessary to analyze odor coding principles in downstream pathways. ORNs expressing the same chemosensory receptor send axons in the olfactory glomeruli where they connect to projection neurons (PNs) in insects and mitral/tuft cells (M/T cells) in vertebrate[29]. Synaptic depression in these first order connections[30] and lateral inhibition[31] mediate by local neurons (LNs) modulate odor representations in the insect antennal lobe[32] (AL) and in the vertebrate olfactory bulb[33]. However a role of these two circuit mechanisms in adaptation has not been investigated so far.

Here we combine computational and experimental approaches in *Drosophila* to understand how ORN adaptive properties shape odor representations in populations of second order olfactory neurons, the PNs. We show that the firing rate adaptation of ORNs is balanced out at their presynapses to ensure an ON-OFF asymmetric background-invariant encoding of the odors, where only the identity of ON stimuli are preserved. Furthermore, we identify the inhibitory feedback mechanism that maintains the ORNs presynaptic calcium tonic and background-invariant. We demonstrate that this invariance can only be achieved if ORNs adapt by shifting their response amplitude, while the classic adaptive shift in sensitivity, predicted by efficient coding theories of single neurons, fails to support asymmetric invariance across backgrounds. Such asymmetric invariance persists in postsynaptic PNs and is disrupted by mutation of a modulatory domain of Unc13, suggesting a role of presynaptic facilitation in achieving the response invariance. We propose that adaptation in ORN firing rates enhances the separation of ON and OFF stimuli in the downstream population of PNs, while allowing a background invariant representation of odor identity for ON stimuli.

Results

Single neuron adaptation shapes odor information coding in ORN populations.

Adaptation has been often described in both peripheral and central sensory neurons as a mechanism that tunes the neuron sensitivity to the stimulus statistics. For example, adaptation to an increasing background luminance, leads to a shift in the response curve of fly photoreceptors towards higher luminances[34]. This shift is consistent with the efficient coding hypothesis[9] and implies that the neuron encodes contrast rather than absolute luminance. ORNs in both insects and vertebrates do not seem to follow the same adaptive strategy as visual neurons[27,28] since they do not exhibit a shift in sensitivity (in the stimulus domain), but rather a decreased response (in the activity domain) after adaptation to an odor background[13,28]. An important difference between vision and olfaction is that stimulus sensitivity across ORNs is highly heterogeneous due to the expression of large odorant receptor repertoires, leading to an early combinatorial encoding of odor information by the ORN population[6,7] (**Fig. 1a**). To understand how single neuron adaptation shapes odor coding at the population level, we simulated the response of a population of ORNs under three different strategies for background adaptation (**Fig. 1b**): I) sensitivity-shift (core mechanism in contrast-sensitive visual neurons), II) amplitude-compression and III) amplitude-shift, the last two being plausible based on measurements in ORNs[13,28]. For each scenario, we simulated the population response to increasing concentrations of a single odor presented in isolation or after adaptation to a background of the same odor type. For all three cases, we described the population responses in a low-dimensional manifold focusing on its capability to encode stimulus properties such as intensity and contrast (relative to the background). If single ORNs adapt by shifting their sensitivity (**Fig. 1c**), the population responses lie on a one-dimensional manifold where the stimulus intensity strongly correlated with the first principal component explaining most of the response variance across all backgrounds (**Fig. 1d**). Background adaptation leads to a slight shift in the representation of iso-intensity stimuli (**Fig. 1d,** black curve). Conversely, the encoding of contrast information in this population is ambiguous, as stimuli with the same contrast can activate very different

ORN configurations (**Fig. 1e,** black curve). Therefore, an adaptive strategy that allows the encoding of contrast in single neurons, leads to population responses that retain mostly information about intensity and not contrast. On the contrary, in a population of neurons that adapt their response amplitude by a compression or a shift, odor representations lay on a 2-dimensional manifold (**Fig. 1f, i**), allowing the parallel encoding of both intensity and contrast information (**Fig. 1g-h and l-m,** black curves). In the fly AL at least two types of neurons receive information from multiple glomeruli, the LNs and the multiglomerular PNs[35–37]. These cell types could in principle encode either intensity or contrast by pulling information from different sets of glomeruli.

Altogether, our results show that adaptation strategies at the single neuron level determine how odor information is represented by the population. Importantly, a strategy that is commonly used at the single neuron level in other sensory systems (strategy I), performs poorly at encoding stimulus features as contrast at the population level, when compared to adaptive strategies that modify response amplitude (strategies II and III).

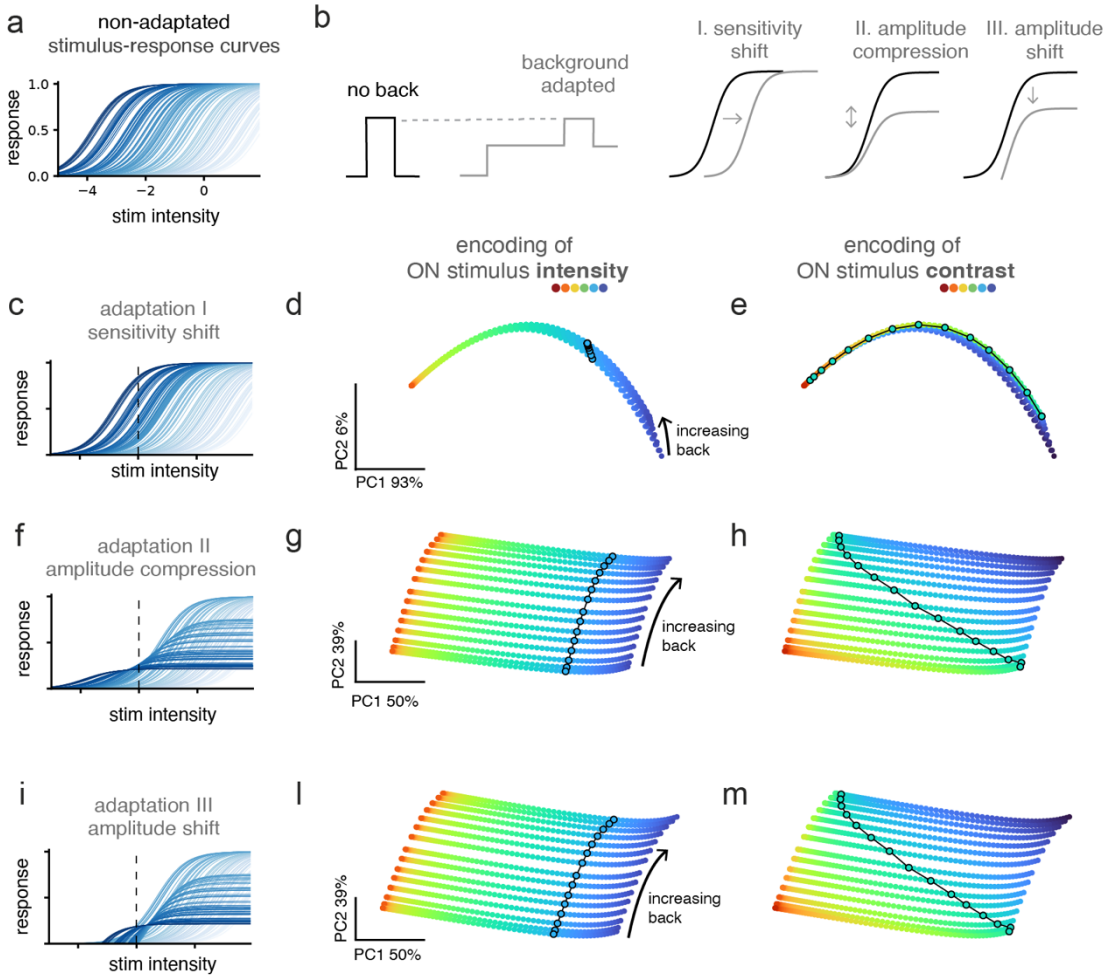

Figure 1. Coding of intensity and contrast in neuron populations with different adaptive properties. a) Simulated stimulus response curves for a population of ORNs with different stimulus sensitivities (stimulus in log scale). **b)** Three types of background-induced adaptation for individual neurons, implemented as a change in a specific parameter for each adaptation case (see Methods). **c)** Response curves of the same neurons as in a) after adaptation to a background stimulus indicated by the dotted line. Adaptation to the background induces a shift of the response sensitivity towards higher stimulus intensities. **d)** 2D-manifold of the population responses to stimuli of different intensity (color coded) in different background adapted conditions. Black circles highlight an iso-intensity response curve across all backgrounds. **e)** Same data as in **d)** but color coded by stimulus contrast. Black circles highlight an iso-contrast response curve across all backgrounds. **f-g-h)** as in **c-d-e)** for a population of

neurons that adapt by a compression in amplitude. **i-l-m)** as in **c-d-e)** for a population of neurons that adapt by shifting their response amplitude.

First and second order olfactory neurons implement a background-invariant representation of ON odor stimuli.

To investigate the computational role of ORN firing rate adaptation, we looked into how these responses are processed in the olfactory glomeruli, where ORNs project their axons. ORNs respond to increasing odor stimuli with phasic firing rate dynamics (**Fig. 2a**). After stimulus onset, the firing rate relaxes to an adapted value, leading to a decrease in the neuron's responsiveness to odor stimuli (**Fig. 2b,c**). Such background dependent responses, typical of adapting neurons, are measured at the dendritic region within the antenna (**Fig. 2d**). Firing activity at the ORN dendrites leads to calcium transients in the corresponding axon terminals within a specific glomerulus in the antennal lobe (**Fig. 2d**). When odor stimuli are presented in isolation, presynaptic calcium transients assayed by fluorescence indicators depend linearly on firing rate (**Fig. 2e**, data adapted from[38]). Surprisingly, these presynaptic calcium responses have tonic and sustained dynamics (rather than phasic as the firing rate) and their amplitude remains invariant across different background concentrations irrespective of firing rates (**Fig. 2f, g**). These striking differences between the dendritic firing rate and the axonal calcium in adapted conditions suggest that presynaptic calcium dynamics are regulated in an activity dependent manner.
To understand the relevance of these observations, we investigated background adaptation in the postsynaptic neurons. ORNs make most of their synapses on uniglomerular PNs. ORN-PN synapses undergo depression on both fast[30] and slow[38] timescales. We reasoned that phasic and adaptive firing rates that impinge onto depressing synapses would result into phasic and adaptive responses in postsynaptic neurons. Contrary to ORNs, PNs calcium dynamics are indeed phasic, but surprisingly their responses to odors are independent of background adaptation, as in the ORNs (**Fig. 2h, i**).

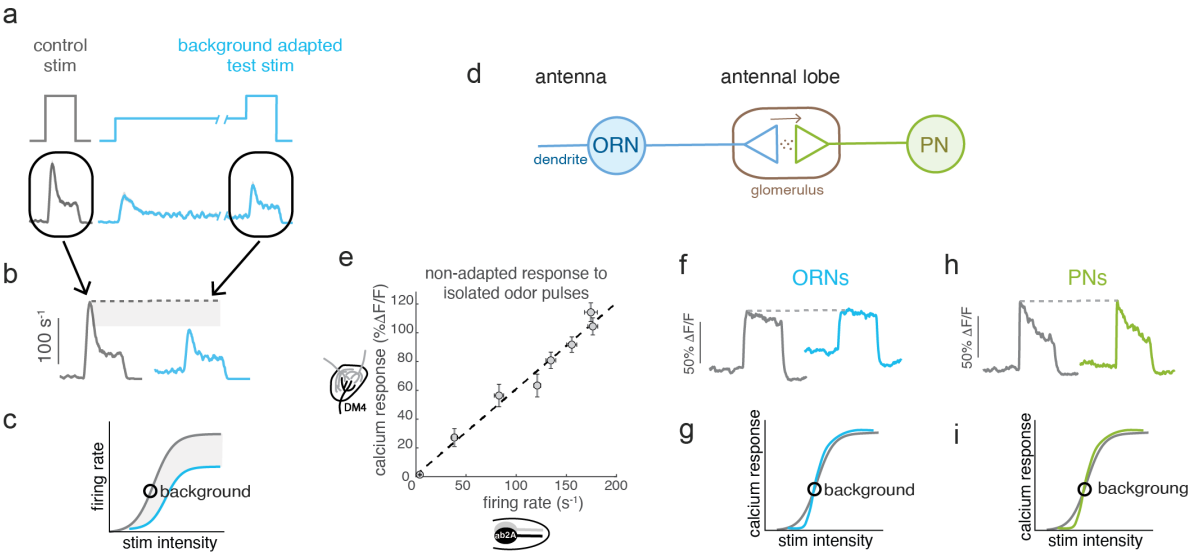

Figure 2. The undoing of firing rate adaptation at central synapses. a) Schematics of the stimulus protocol and firing rate response of the ORNs in control and background adapted conditions (ab2A**,** data adapted from[38]). **b)** Comparison between the response in control and background adapted conditions, showing a decreased response after adaptation. **c)** Schematics of the ORNs response curve quantified from firing rate measurements in control and background adapted conditions. The circle indicates the intensity of the background stimulus. **d)** ORN located in the antenna extend their axons to a specific glomerulus in the antennal lobe and make synapses on uniglomerular PNs. **e)** Mean firing rate and calcium responses to isolated odor puffs of different intensity (data from[38]). The blue line indicates a linear regression. Error bars indicate SEM. **f)** ORN calcium responses induced by an odor puff in control and adapted conditions measures from the ORN axon terminals (glomerulus DM1). **g)** Schematics of the ORN calcium response curve showing background-invariant responses. **h)** PN calcium responses in control and adapted conditions

measure from the same glomerulus as in **f)**. **i)** Schematics of PNs calcium response curve showing background-invariant responses.

To validate the generality of this observation, we explored a range of ON and OFF stimuli, i.e. odor pulses higher or lower than the adapting background stimulus (**Fig. 3a, b**). PN responses to ON stimuli had similar amplitudes independently of background adaptation (**Fig. 3a and Fig. S1a**), also for high background concentrations (**Fig. S1b).** In contrast, OFF stimuli, even of small amplitude, always produced large and fast decreases in calcium (**Fig. 3b and S1b, c)**. To capture the transition between ON and OFF responses irrespective of experimental noise in the generation of the stimuli, we analyzed single trials by defining *contrast* the relative difference between the response to the control pulse and the adaptive background, and *relative adaptation* as the fold change in the response to the pulse between control and adapted conditions (**Fig. S1c)**. Zero contrast means that the tested stimulus equals the background, and zero adaptation means that PNs respond in a background-invariant manner. By binning the single trials based on contrast value, one can capture the sharp transition between ON and OFF stimuli (**Fig. 3c**), which demonstrates almost perfect background-invariance only for ON stimuli in the PN dendrites. Responses to OFF stimuli instead fall much below the non-adapted response also for very small contrast values. We refer to this encoding property of the olfactory system as *asymmetric background-invariance*. These results contrast with a previous report of background adaptation in PNs firing rate[40]. This incongruency could be due to the lack of a precise odor delivery system. To corroborate our finding with a different method, we performed voltage recordings in the dendrites of PNs. Using PN-specific expression of the voltage sensor ASAP2s[39], we fshow that PN dendrites depolarize similarly or even slightly more (rather than less) when odor stimuli are presented on a background (**Fig. 3g-h**), in agreement with the calcium measurements.
Therefore, both ORN presynaptic and PNs postsynaptic activities encode a background-invariant representation of ON odor stimuli despite background dependent ORN firing rates[12,13] and strongly depressing ORN-PN synapses[30,38].

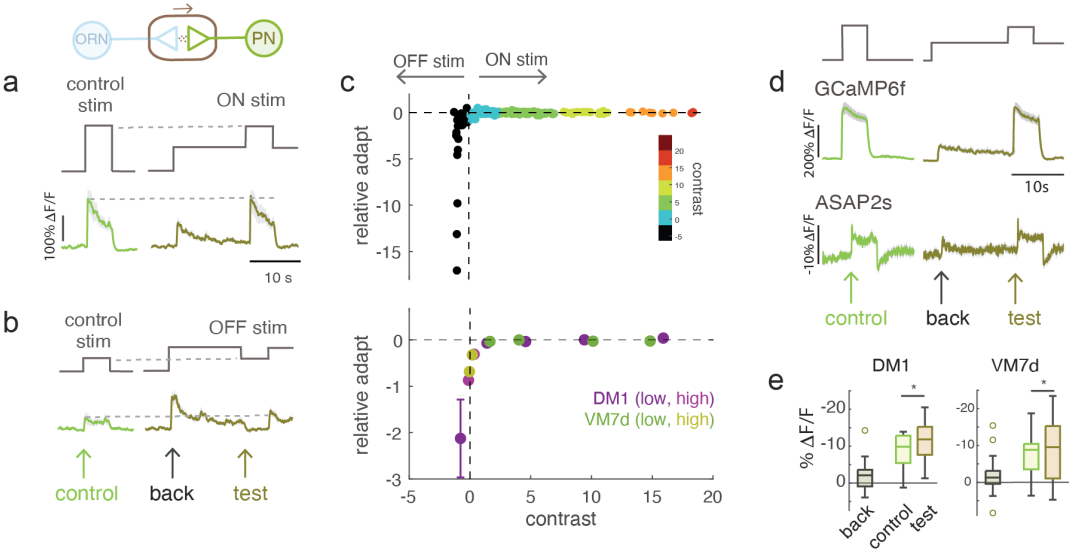

Figure 3. Asymmetric background-invariance of PN responses. a, b) Schematics of the stimulus protocol and calcium responses of PNs withing glomerulus DM1 for two examples of ON and OFF stimuli. Lines indicate the mean ΔF/F, shaded area sem, N=9-11. **c)** *Top:* Relative adaptation as a function of contrast for each single trial, including two independent datasets recorded from two different glomeruli. Data are color coded by contrast; black indicates OFF responses. *Bottom*: relative adaptation averaged in bins of contrast; color coded by glomerulus type. *Low* and *high* indicate two different datasets where different ranges of background concentration where used (N=9-11, see also **Fig. S1**). **d)** Control and background adapted response measure in DM1 using either a calcium or voltage sensor. Thick lines indicate the mean ΔF/F and the shaded areas sem. Liquid dilution of methyl acetate is 10^{-4} for the background and 10^{-2} for the pulse. **e)** Boxplot representing median, quartiles, min/max values and outliers of ASAP2s signals from two glomeruli. (DM1 N=19, VM7d N=23, *p<0.05, Kruskal-Wallis).

Background-invariant ORN presynaptic activity is a glomerulus-intrinsic property.

Odor stimuli can recruit more than one ORN type, raising the question of whether the background invariance of ORN presynaptic response depends on inter-glomerular inputs. We used an optogenetic approach to restrict activation to a single ORN type (expressing *Or42b*) targeting the glomerulus DM1 (**Fig. 4a**). Using a combination of background and test stimuli, we show that as with odors, ON stimuli elicited the same response irrespective of background, while OFF stimuli always lead to quick drops in calcium (**Fig. 4b, c**). We additionally measured firing rates from the ab1 sensillum that contains the *Or42b*-ORNs to verify background dependent responses (**Fig. 4d**). Optogenetic activation leads to lower firing rates and a smaller dynamic range compared to odor stimuli (response saturates at around 40 Hz rather than the usual 250 Hz). Yet, as with odors, background adaptation leads to a striking change of the dose-response curve for both ON and OFF stimuli (**Fig. 4d**). We conclude that presynaptic calcium is regulated in a glomerulus-intrinsic manner such that both uni- (**Fig. 4**) and multi-glomerular (**Fig. 2, 3**) odor representations are normalized to achieve asymmetric background-invariance.

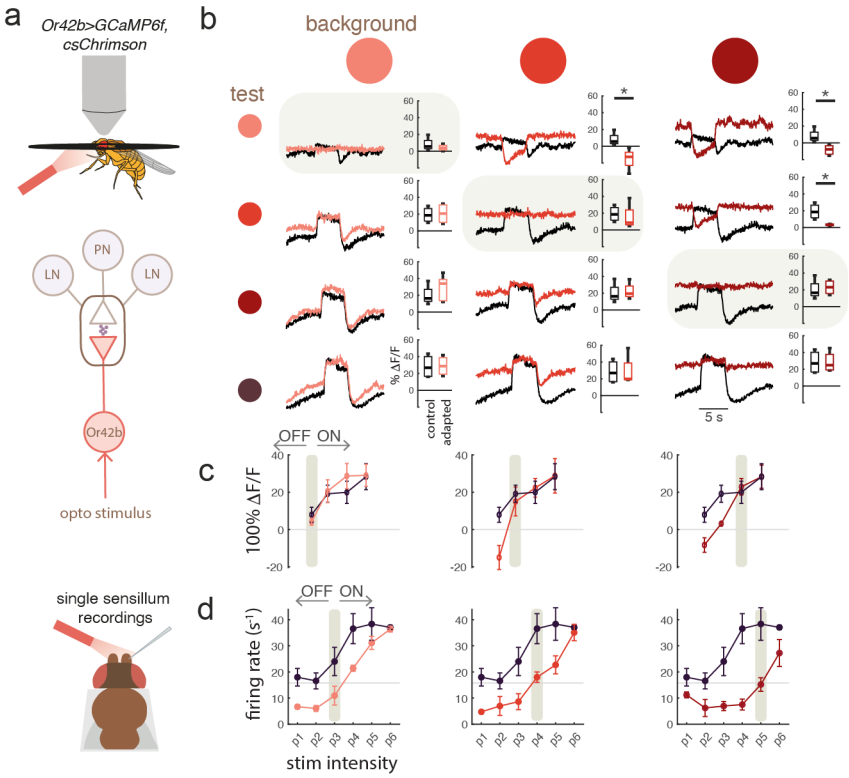

Figure 4. Asymmetric background-invariance in ORN upon optogenetic activation. a) Schematics of the experimental protocol. **b)** Mean calcium responses from ORN axon terminals in the glomerulus DM1 in control (black, no background) and adapted (shades of red) conditions. Columns represent different background intensities, rows different intensities of the test stimulus. Test intensities ranged from 0.01 to 0.08 µW/mm^2 (from light to dark red). The plots on the diagonal (gray quadrants), corresponds to the same intensity of the test and background stimuli. Quadrants above this diagonal, are OFF stimuli and quadrants below are ON stimuli. Boxplots show median, quartiles and min/max values of the response averaged in 3 sec after stimulus onset (N=4-5, *p<0.05). **c)** Mean response plotted as a function of the test stimulus intensity; error bars indicate sem. **d)** Same as **c)** but for firing rate responses (N=3). A similar range of stimuli was used for the electrophysiology (0.06-0.92 µW/mm^2). Gray boxes indicate the intensity of the background stimulus.

Homeostatic feedback regulates ORN presynaptic calcium responses.

Next, we investigated the potential mechanisms that allow ORN to compensate the firing rate adaptation and achieve ON background invariance. Specifically, we asked whether ORN presynaptic calcium is regulated in a cell-intrinsic manner or through a circuit computation. To separate between these two cases, we expressed the temperature-sensitive dynamin mutant shibire^{ts} in *Or42b*-ORNs to block neurotransmitter release and measured odor responses at the same presynapses (**Fig. 5a**). In this condition, the presynapses can still receive lateral inputs from other glomeruli activated by the odor (e.g. DM4). To capture slower adaptive processes, we presented the test odor concentration 8 consecutive times (**Fig. 5b**). As expected, flies of the control genotype showed tonic and background-invariant responses (**Fig. 5c**). In contrast, blocking synaptic release led to more transient and background dependent responses (**Fig. 5d-f**), reminiscent of firing rate adaptation (**Fig. 2a, b**). Similar results were obtained for the glomerulus DL1 (**Fig. S2a-d**). Therefore, synaptic output of an ORN type is required to maintain its presynaptic calcium background-invariant.

ORN synapses release acetylcholine in the AL. Pharmacological block of acetylcholine receptors (ACh-Rs) also led to transient and background-dependent responses (**Fig. 5g-l**) for different combinations of test and background stimulus (**Fig. S3a-c**), further indicating that the regulation of the pre-synaptic calcium is not a cell-intrinsic property and requires a synaptic feedback loop. ORNs make most of their synapses with PNs and local neurons (LNs). Genetically silencing PN synaptic output had no effect on presynaptic calcium in ORNs, excluding an output gain control mechanism (**Fig. S2e-f**). LNs form a diverse population of inhibitory neurons mediating different types of gain control in the AL[32,41], but their role in the context of background adaptation remains unexplored. Pharmacological block of GABA receptors led to similar effects as blocking of ACh-Rs (**Fig. 5m-p, and Fig. S3g-i**), suggesting that GABAergic LNs play a major role in tuning background adaptation in this glomerulus.

However, this might not be the only mechanism across the entire ORN population. ORNs innervating glomerulus DL5 also have background-invariant responses (**Fig. S3d**), although they reach perfect invariance only after the first 3 odor pulses (**Fig. S3e**). DL5 also differs from DL1 and DM1 in its baseline calcium, which slowly increases across stimulus repetitions creating a slow ramp in the response (**Fig. S3d**). Blocking of acetylcholine (and GABA) receptors did not drastically affect background invariance of DL5 calcium response and did not eliminate the baseline increase in calcium (**Fig. S3d-f and S3j-l**). This different effect of the pharmacology is unlikely due to drug penetration, because the data were acquired from the same preparation, on the same focal plane and with the same stimuli as for DL1.

Overall, our data indicate that at least in some glomeruli, inhibitory inputs on the presynapses mediate a form of input gain control that counteracts firing rate adaptation making ORN responses to ON stimuli background-invariant. Other glomeruli implement an alternative strategy that likely does not require circuit feedback and might rather rely on a cell intrinsic homeostatic control of pre-synaptic calcium.

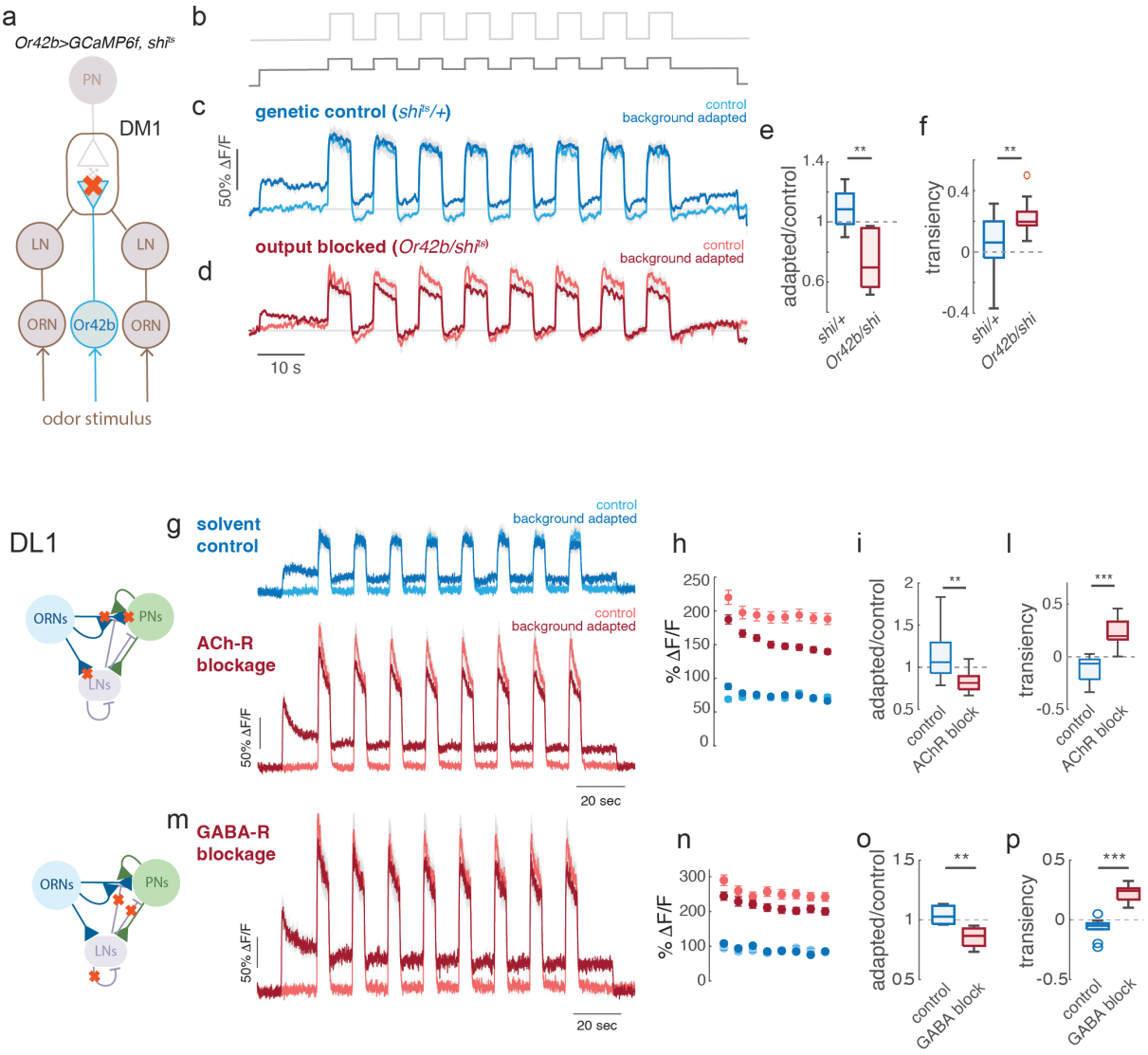

Figure 5. An input gain control mechanism maintains ORN presynaptic calcium background-invariant. a) Genetic blockage of or42b-ORNs neurotransmitter release. **b)** Stimulation protocol in control (light gray) and background adapted conditions (dark gray). **c)** Calcium response of the DM1 glomerulus in genetic control flies showing background-invariant responses. **d)** Calcium response in flies with blocked ORN synapses showing background dependent responses. **c-d)** Methyl acetate liquid dilution of 10^{-4}. Background airflow dilution C5 and pulse C6 (see **Table S3**). **e)** Relative adaptation measure as the response ration in adapted and control conditions. **f)** Response transiency measured as the relative change in response at stimulus onset and offset (transiency=1-f_{OFF}/f_{ON}, N=7,8). **g)** Calcium responses from the DL1 glomerulus before and after drug application. Pure 2-butanone was used in airflow dilutions of C7 for the background and C8 for the pulse. For the blockage of AChR 100 µM atropine + 20 µM tubocurarine + 200 nM imidacloprid (N=10). **h)** Mean response to the single pulses, **i-j)** as in **e-f)**. **m-p)** as **g-l)** for GABA-R blockage: 25 µM CGP54626 + 5 µM picrotoxin (N=5). Thick lines indicate mean and shaded areas indicate SEM. Box plots indicate median, quartiles, min/max values and outliers. **p<0.01, ***p<0.001, Kruskal-Wallis.

An amplitude-shift adaptation mechanism is required to achieve background invariance through inhibitory feedback.

We next asked how inhibitory feedback from the LNs can lead to invariant calcium dynamics across different background conditions. To address this question, we implemented a circuit-model of ORN calcium responses in which ORN firing rates provide the excitatory inputs while LN responses drive the inhibitory feedback loop (**Fig. 6a**). To achieve asymmetric invariance across all background conditions, we show that the adaptation mechanism must act as a differential operator in the response

domain, equivalent to the amplitude-shift adaptation (see Methods). Assuming a functional form for the ORN response as in **Fig. 1**, we explicitly modeled the calcium responses of ORNs for the three different adaptation mechanisms in **Fig. 1b** (see further details in the Methods). The sensitivity-shift mechanism ensures an invariant calcium response in a test dependent manner, for which information about both the test and background stimuli are required. As a consequence, calcium responses after adaptation to different backgrounds are invariant only for a specified test stimulus (**Fig. 6b,** dotted line). Similarly, the amplitude-compression mechanism leads to a test-dependent response that ensures invariance only for stimuli much higher than the background (**Fig. 6c,** and Methods). As predicted, only the amplitude-shift adaptation mechanism ensures invariant calcium responses for all backgrounds and test stimuli (**Fig. 6d**).

Altogether, we demonstrated that an inhibitory feedback can mediate ON background invariance only if the input firing rate adapts with an amplitude-shift mechanism, highlighting a new computational role of adaptation that deviates from efficient coding predictions at the single-neuron level.

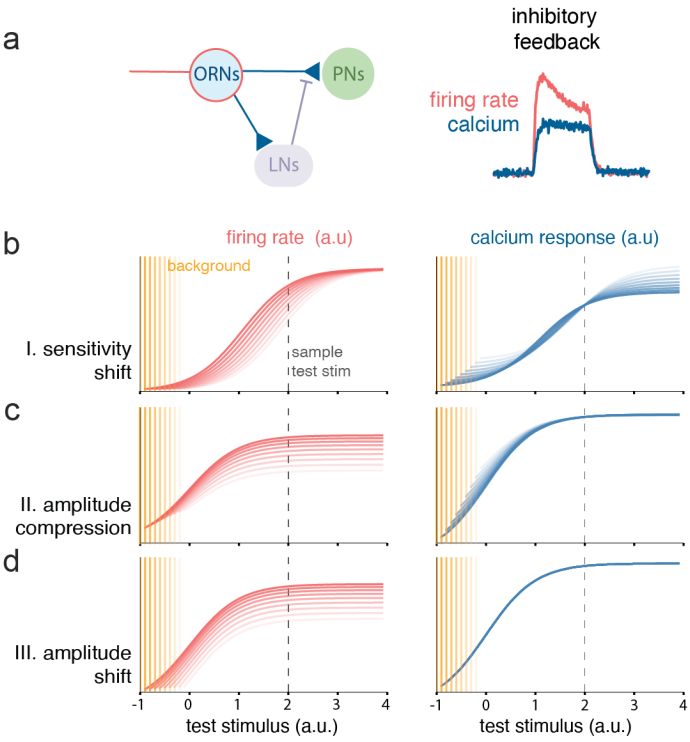

Figure 6. Adaptation mechanisms for background-invariant response. a) We consider an inhibitory presynaptic feedback loop with ORN firing rate as input and ORN axonal calcium as output. **b-c-d)** Firing rate and calcium response for three different adaptive functions: sensitivity-shift, amplitude-compression, amplitude-shift. Orange lines indicate the value of the adaptive background stimulus. Curves with different shades of red/blue correspond to different adapted conditions. Dotted lines indicate a representative test stimulus.

Background invariance of PN responses requires modulation of ORN synaptic release.

Next we investigated the link between tonic and background-invariant presynaptic calcium and background-invariant postsynaptic response of the PNs. We reasoned that tonic levels of presynaptic calcium might be associated with enhanced engagement of the neurotransmitter release machinery (**Fig. 7a**). Synaptic potentiation might occur through several, possibly redundant, pathways. Conserved Unc13 proteins are essential for synaptic transmission from the release sites to which vesicle fusion is restricted and mediate several types of presynaptic plasticity (e.g. short-term facilitation and homeostatic potentiation) [42–48]. Two different splicing variants, Unc13a and Unc13b, are differentially organized at the ORN-PN synapses and mediate different postsynaptic currents[49]. Unc13 proteins contain three functional domains that can be modulated directly or indirectly by calcium: the

Ca^{2+}/calmodulin binding CaM domain, the C1 domain binding diacylglycerol (whose metabolism is Ca^{2+}-dependent), and the C2B domain, that binds phosphoinositides in a Ca^{2+}-dependent manner[42,50]. The C1 and C2B domain were shown to exert autoinhibition on the vesicle priming reaction which makes vesicles responsive to action potentials[51]. Activation of the Unc13-C1 domain enhances action-potential induced transmitter release and diminishes multiple forms of presynaptic plasticity (i.e. short-term facilitation, post-tetanic potentiation, and homeostatic potentiation)[52–54]. A single amino acid exchange (H→K) in the C1 domain reconstitutes this enhanced potentiation [53,55]. We hypothesized that this gain of function mutation might interfere with presynaptic plasticity required to achieve background invariance. We therefore introduced the corresponding Unc13 mutation (H1723K, see Methods) into flies and tested three stimulus conditions combining two concentrations of the background and test stimulus (**Fig. 7b**). In control flies, all three stimulus conditions led to background-invariant responses in DL5 ORNs and PNs (**Fig. 7b, c**). It should be noticed that in this glomerulus background invariance is not yet achieved at the first pulse tested, which gives a higher response in background adapted conditions in both ORNs and PNs. However, perfect background adaptation is achieved at the second odor pulse. Such invariance was lost in Unc13-C1 mutants for two of the three stimulus conditions tested (**Fig. 7d**). We did not see major effects of the C1 domain mutation for the high contrast condition, which indicates that the calcium modulation probably involves more than one mechanism. Comparing control and mutant flies across three different glomeruli (including DL1 and DM4), we observed significant effects of the mutation on relative adaptation for two of three of the stimulus conditions tested in each glomerulus (**Fig. 7e**). The mutation specifically affected the response to background adapted stimuli while it had no or mild effects on the response in non-adapted conditions, indicating that only activity-dependent modulation of the domain is disrupted, while synaptic transmission itself is not impaired or attenuated (**Fig. 7f**).

Overall, we conclude that modulation of Unc13 is necessary to keep PN postsynaptic response background-invariant and stable over time. This pathway might act redundantly or synergistically with other calcium-dependent modulations of presynaptic function.

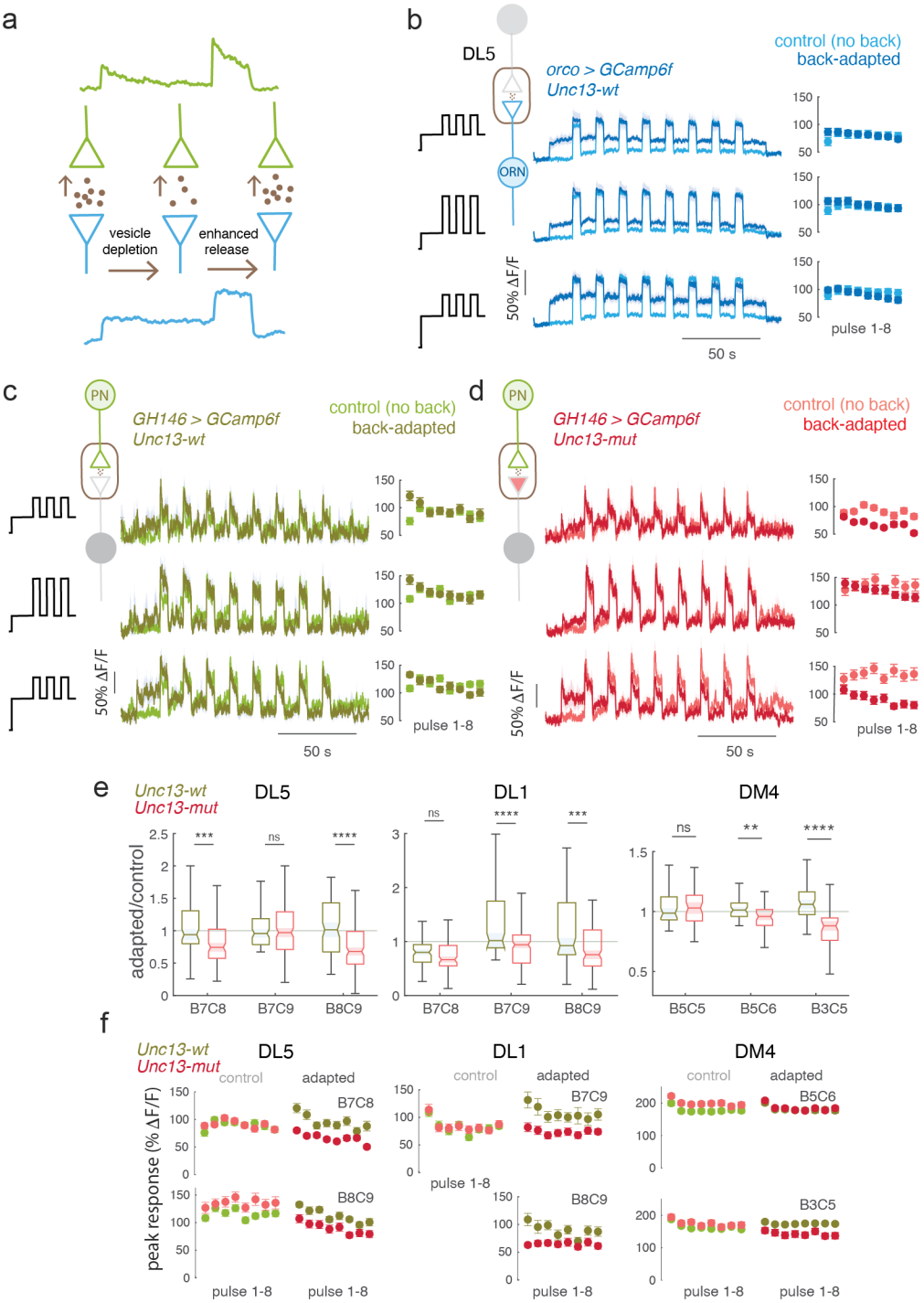

Figure 7. Unc13 C1 domain is required for background-invariant PN response. a) Schematics of model hypothesis. **b)** Mean calcium response from ORN axon terminal to 8 odor pulses in control and adapted conditions for three combinations of background and test stimuli. Shaded areas indicate sem. Right, quantification of the mean response to each odor pulse. **c,d)** same as **b)** for PNs in control and Unc13 C1 mutant flies (WT N=6-7, mutant N=7-11). **e)** Background adapted response divided by the control for each stimulus condition tested in three different glomeruli. For DL5 and DL1, pure 2-butanone was used. A methyl acetate liquid dilution of 10^{-4} was used for DM4. Bar plots are generated from all flies measured and all 8 puffs in each trial (DL1: control N= 6-7, mutant N=7-11, DM4: control N= 6-8, mutant N=6-7). Bar plots indicate median, notch, quartiles, max and min. **f)** Mean peak response for control and Unc13 C1 mutant flies for 8 consecutives odor puffs in control adapted conditions. Error bars indicate sem.

A population code with asymmetric background invariance

The implementation of an adaptation strategy that shifts the amplitude of the response curve allows ORN to compensate firing rate adaptation and achieve a background-invariant representation of ON stimuli (**Fig. 6**). To understand the consequences of this asymmetric invariance in the downstream population code, we implemented a model of PNs at both the single-neuron and population level. For single PNs, we observed a relative adaptation curve that exhibits a sharp but continuous transition from ON to OFF contrast stimuli (**Fig. 3c**). We attribute this smooth transition to a small signal to noise ratio near the range of zero contrast that we can reproduce by including Gaussian noise in the adaptation response of PNs (**Fig. S4**, and Methods). We then used this model to compare the encoding of ON and OFF stimuli in populations of ORNs and PNs. A population of ORNs encodes both intensity and contrast information (**Fig. 1**, only ON stimuli) with a smooth transition from ON (colored) to OFF (black) stimuli (**Fig. 8a, b**). In contrast, the response space of the PN population exhibits a discontinuity that separates ON and OFF stimuli across different backgrounds while preserving a background-invariant representation of ON stimuli (**Fig 8c**).

Since the background invariant responses of PNs do not encode contrast explicitly at the population level, there is a remaining question of why ORN populations should encode this feature (**Fig. 1**). We have shown both experimentally (**Fig. 3**) and computationally (**Fig. 6**) that firing rate compensation can be performed in a glomerulus intrinsic manner. However, when multiple glomeruli are active, background invariance must be achieved in a coordinated way across the AL. It is known that LNs mediate a form of normalization that relaxes the non-linearity in the ORN-PN transformation[32]. This normalization is mostly presynaptic[32,56] and relies on a measure of overall activity across receptor types, which as we have shown can encode both intensity and contrast (**Fig. 1**). We studied the effects of such normalization by including an interglomerular LN to the local ORN-PN circuit (**Fig. 8d** and Methods). We observe that adding this interglomerular normalization factor enhances the encoding of low contrast stimuli (**Fig. 8e**). We show that ON background invariance of the PNs response can still only be achieved by the amplitude-shift mechanism if interglomerular LNs encode contrast information extracted from the ORN population (**Fig. 8c** and Methods). In the absence of background stimuli, the encoding of contrast equals the encoding of intensity which is in good agreement with reported function of the LNs[32]. Therefore, our model incorporates previously known computations of the AL network generalizing them to the context of background adaptation.

Overall, we conclude that the AL implements a circuit computation that extracts contrast information encoded in ORNs to enhance the discriminability between ON and OFF stimuli in postsynaptic PNs while still preserving information of odor identity for ON stimuli.

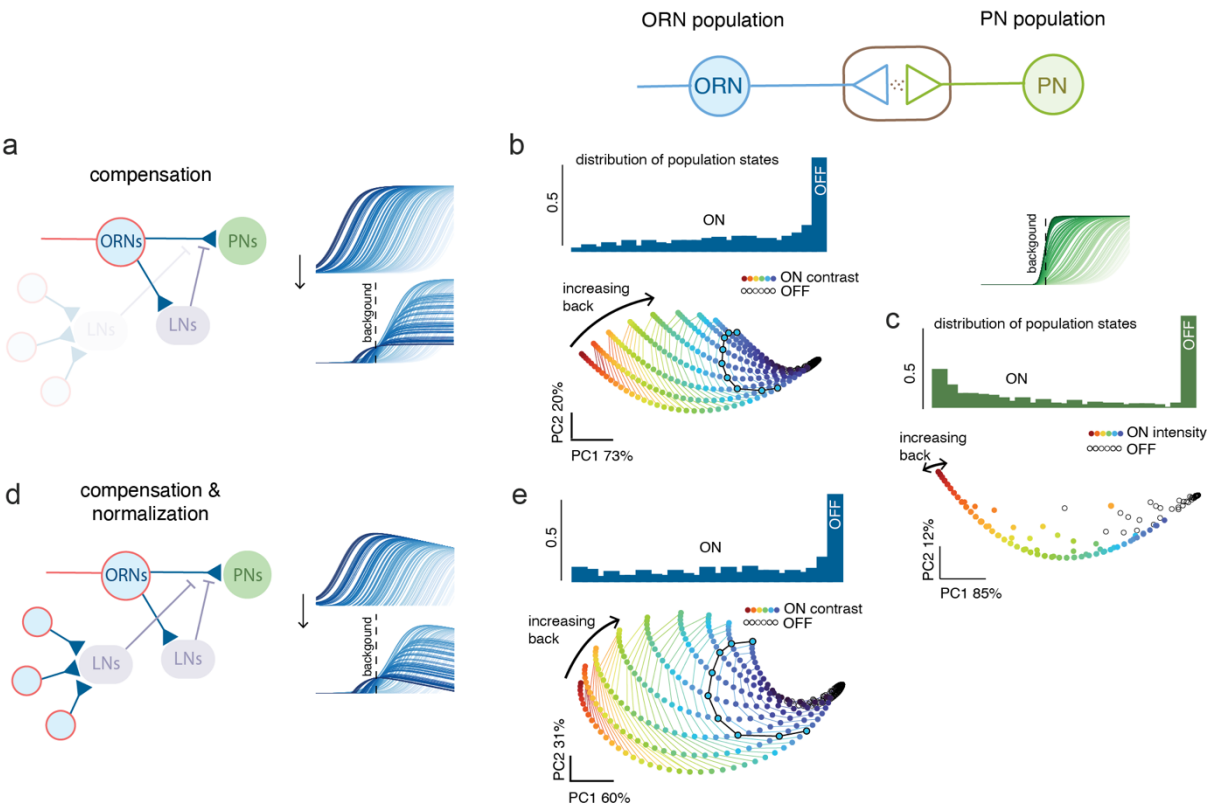

Figure 8. Combinatorial representation of ON and OFF stimuli in ORN and PN populations: a) Schematics of the circuit model that implements synaptic compensation of firing rate adaptation. *Right*: firing response curves for a population of ORNs with different stimulus sensitivities in control (*top*) and background adapted conditions (*bottom*). **b)** 2D-manifold of the population response to stimuli of different ON (color coded) and OFF (black) contrast in different background adapted conditions. The histogram represents the distribution of population states calculated on the first principal component. **c)** Same as **b)** for PNs, but responses are color-coded by stimulus intensity. PNs ON background-invariance was modeled as described in **Fig. S4**. **d)** Schematics of the circuit model that implements both synaptic compensation and interglomerular normalization. *Right*: response curves for a population of ORNs with different stimulus sensitivities in control (top) and background adapted conditions (bottom). **e)** Same as **b)** but responses of single neurons are normalized by a term proportional to stimulus contrast.

Discussion

Odors are detected by single sensory neurons that work combinatorially to represent complex natural stimuli at the population level. Despite the key role of adaptation for information coding in both single neurons and neuronal populations, the adaptative properties of the olfactory system have been largely overlooked. In this work, we investigated adaptation as a coding strategy of single ORNs that shapes the encoding capabilities of olfactory neural populations. By combining experiments and computational models, we identified a novel property of the olfactory pathway that we defined as asymmetric background invariance. We show that the adapted responses of single ORNs are reset to achieve an asymmetric representation of ON and OFF contrast stimuli, where ON responses are background-invariant while OFF responses collapse in the representation space of the downstream populations. We find that a presynaptic inhibitory feedback and synaptic potentiation mediate this transformation, which enhances the separation of ON and OFF stimuli and preserves information on the identity of ON stimuli necessary for downstream computations.

The role of adaptation at the single neuron and population level.

Efficient coding principles provide an explanation for how single neurons adapt their response function to changes in stimulus statistics[9]. Similar principles have been used to understand how the response function of neurons in a population should adjust to tile the stimulus space in a flexible manner[57]. This

is of particular importance to understand coding principles in the olfactory system, which uses a repertoire of receptors to detect and discriminate odors. Receptor repertoires strongly adapted, through evolutionary times, to the ecology of the animal[58], leading to efficient sensory codes in the ecological relevant stimulus space[59]. A similar adaptive strategy also applies on shorter timescales. For instance, the expression levels of the receptors are plastic in mammals, providing a mechanism to optimize the composition of a receptor repertoire to changes in the environment[60].

Similar adaptive changes in the coding capability of a receptor repertoire could in principle occur also on shorter time scales, but there is limited evidence of such a strategy in the olfactory system[27]. In this work, we provided evidence that the fly olfactory system does not adapt the odor representation to the background. Rather, it implements mechanisms that keep odor representations robust with respect to changes in the background. While efficient coding theories of single neurons predict the conventional sensitivity-shift strategy widely observed in the visual system, both ORNs and PNs do not follow this principle. ORNs adapt by shifting their response amplitude (and not their sensitivity) which ensures the compensation necessary to achieve ON background invariance in downstream neurons, the PNs. Therefore, even though a persistent stimulus (the background) induces synaptic depression and a corresponding decrease in postsynaptic activity[38], it also primes the synapses to respond to ON stimuli as strongly as in absence of background.

Our findings raise the question of why would ORNs adapt at all if the goal is to encode absolute stimulus intensities. We argue that firing rate adaptation is beneficial to the asymmetric encoding of ON and OFF stimuli, where only ON stimuli preserve stimulus identity, while OFF stimuli collapse into a low-response state. Such asymmetry would not be possible if the ORNs simply encoded stimulus intensity. From a more speculative perspective, another potential benefit of adapting firing rate and then compensating it downstream, could be that of lowering the total energetic cost of sending information through the brain with no information loss. However, further work is necessary to assess whether the synaptic computations that compensate firing rate adaptation are indeed less energetically costly than implementing a non-adaptive spiking code.

The role of asymmetric odor encoding downstream of PNs.

PNs send odor information to both the LH and MB, contributing to higher order computations. Odor representations in the Kenyon cells (KCs) of the MB are used to form associative memories based on the co-occurrence of an odor and a reinforcement[61]. For memory retrieval, it is critical that the same KCs are activated by the conditioned stimulus in training and test phase and therefore it is critical that the odor is represented independently of possible backgrounds. Altogether, memory retrieval provides a potential function for background-invariant encoding in PNs. Consistently with this hypothesis, a recent study showed that locusts learn in a background-invariant manner[62], suggesting that the MB has access to a background-invariant representation of odors.

Odor cues are used not only to evaluate, but also to explore the environment. Animals use odor gradients[63,64], plume statistics[65,66] and odor motion[67] to direct their behavior in complex olfactory environments. These computations require the detection of gradients and contrast in an odor specific manner. It is plausible that such computations do not occur in the AL where odor representations are formed, but in downstream neurons that can read out a population response from the AL to then compute stimulus specific information on contrast. The LH provides the cellular complexity[68,69] to perform odor-specific computations in parallel[70], including the encoding of contrast[71]. We suggest that the encoding of background-invariant ON responses through the compensation of ORNs adaptation is essential for downstream stimulus-specific computations that drive key behaviors in flies. These computational requirements do not generalize to OFF stimuli, which have a very different relevance for the fly behavior compared to ON stimuli, leading to an explorative search rather than an oriented behavior [63,72].

Cell intrinsic and circuit mechanisms that maintain ON stimulus invariance.

Asymmetric background invariance is the most robust observation we made across all our measurements in both ORNs axons and PNs dendrites. However, we also encountered differences across glomeruli. First of all, ORN calcium dynamics range from being slightly phasic (DM1), completely flat (DL1), to slightly ramping up (DL5). This seems to correlate with background

invariance to be achieved already on the first (DM1), only on the second or third (DL1, DL5) odor pulse. Moreover, we showed that ORNs' background invariance in DM1 and DL1 requires synaptic transmission, while DL5 background invariance does not. This indicates that cell intrinsic mechanisms might be implemented in DL5, which could involve the regulation of internal calcium storages[73,74].
In all tested glomeruli, we find that a gain of function mutation of the Unc13-C1 domain occludes PNs background invariance. So far, we do not have direct evidence that plasticity involving Unc13 is mediated by the tonic and background-invariant presynaptic calcium nor that it is downstream of lateral inhibition. However, our current working model postulates a link between presynaptic calcium regulation and synaptic facilitation. As the Unc13 mutant does not abolish background invariance for all stimulus conditions, other calcium dependent mechanisms are likely involved in this plasticity, perhaps through modulation of other synaptic proteins such as synaptotagmins[75].
Overall, we conclude that synaptic facilitation is a key mechanism for PN background invariance and that molecular pathways usually studied in the context of homeostasis are involved in this adaptive computation. At ORN-PN synapses the homeostatic set point is the non-adapted response. Differently from other models of synaptic homeostasis, the feedback compensation is not calculated based on synaptic output (PN response) but based on the input drive to synaptic release (ORN firing rate). This synaptic strategy is to our knowledge unique in its design and perhaps specific to the computational demands of the olfactory system.

The undoing of a neural computation: evolutionary considerations

Undoing an upstream computation is rather an uncommon observation that becomes counterintuitive from an efficient coding perspective, where computations are expected to optimize information processing across neuronal layers. However, if we look at neural circuits as ongoing projects of evolution rather than fully optimized systems, more examples of undoing can be found. For example, some amacrine cells in the visual system undo the color opponency calculated in upstream neurons to preserve the balance between opponent and non-opponent units in the retina[76] such that both types of information are transferred in downstream neurons. The logic of this computation could result from the order in which these mechanisms evolved (discussed in[76]).
From an evolutionary perspective, the olfactory system is designed to ensure adaptability which is implemented primarily by the evolution of chemosensory genes. Our considerations focused on the combinatorial aspect of odor coding, and therefore the fact that stimuli are encoded in populations of sensory neurons, with identity defined by the OR they express. However, this system evolved from an ancestor that expressed only one or few ORs[77]. In such a low dimensional system, firing rate adaptation might not only have been parsimonious, but also an efficient strategy for odor encoding, as it is the case of visual neurons. Only after the emergence of a combinatorial coding strategy with multiple ORs, the olfactory system might have selected for mechanisms that support background invariance.
Olfactory systems also evolved specialized channels that encode unique chemicals, such as pheromones[78] or harmful substrates[79], crucial in certain ecological contexts. These stimuli therefore do not rely on a population code and might implement different strategies for adaptation. A combination of mechanisms can be therefore expected within the same sensory system depending on the function of specific subcircuits. Further insight into these questions might benefit from the study of downstream areas like the LH that read out combinatorial or specialized representations for behavioral-relevant computations.

Material and methods

Experimental model / fly husbandry

All flies were kept on a standard molasses-based food at 25°C and on a 12h:12h light-dark cycle or at room temperature in the laboratory. For optogenetic experiments, flies were kept in the dark and on food that was supplement with 1mM all-trans retinal (Sigma-Aldrich, Table S1) for at least 4 days before experiments. For shibire^{ts} experiments, flies were incubated for at least 1h at 36-37°C before the start of recordings, which lasted a maximum of 45min. Female flies were used for all experiments. The complete genotypes are given in Table S2.

524
525 **Fly mutagenesis Unc13 C1 HK**
526 The mutation of the Unc13 C1 domain was based on the corresponding mutation of the mouse
527 homologues Munc-13-1 where histidine 567 was changed to lysine[53]. Sequence alignment with
528 *Drosophila* Unc13A identified histidine 1723 as the relevant target. Note that the two *Drosophila* splice
529 isoforms Unc13A and Unc13B harbor a C1 domain[48] and that this modification therefore affects both.
530 CRISPR-mediated mutagenesis was performed by WellGenetics Inc. using modified methods of Kondo
531 and Ueda[80] to generate a break in unc-13/CG2999. A PBacDsRed cassette containing two PBac
532 terminals and 3xP3-DsRed and two homology arms with point mutations (one to induce the amino acid
533 change and one to introduce a TTAA sequence to recognize proper integration on the other homology
534 arm) were used for repair. The DsRed marker was intermittently used to identify flies with successful
535 integration events in the F1 generation. The marker was later excised and the presence of the point
536 mutation and successful removal of the cassette in the final fly line validated by PCR and sequencing
537 from genetic DNA.
538
539 ***In vivo* calcium imaging**
540 Flies 6-10 days post-eclosion were anesthetized on ice and mounted on a custom holder using the
541 Bondic repair system (Bondic cartridge with Bondic liquid plastic and Bondic UV-LED). The proboscis
542 was secured and the maxillary palps were covered using low melting temperature wax. Saline solution
543 (5mM Hepes, 130 mM NaCl, 5mM KCl, 2 mM MgCl2, 2mM CaCl2, 36 mM Saccharose – pH 7.3) was
544 added and the cuticle covering the fly's brain, as well as obstructing trachea and fat tissue, were
545 removed.
546 Functional imaging was performed on an Investigator two-photon microscope (Bruker) coupled to a
547 tunable laser (Spectraphysics Insight DS+) with a 25×/1.1 water-immersion objective (Nikon). Laser
548 excitation was tuned to 920 nm, and less than 20 mW of excitation was delivered to the specimen.
549 Emitted light passed through a SP680 short-pass filter, a 560 lpxr dichroic filter and a 525/70 filter.
550 PMT gain was set to 850 V. The microscope was controlled with the PrairieView (5.4) software.
551
552 **Stimulation**
553 Test and control stimuli were 5 sec long, background stimuli were 15 sec. In Fig. 4,5,6 test and control
554 stimuli were repeated 8 times with 10 sec between repetitions.
555 Optogenetics: light from a 625 nm LED was directed to the fly's antenna using an optic fiber. The LED
556 was controlled by the imaging software and activated during the laser flight-back, allowing
557 simultaneous acquisition and excitation. In electrophysiological experiments, the LED was controlled
558 by an Arduino board.
559 Odor delivery: a flow of clean air was presented to the fly continuously (1L/min). To this main airflow,
560 either an odor (odorant airflow; 100mL/min) or more clean air (balancer airflow; 100 mL/min) was
561 added through a solenoid valve (LEE), so that the final airflow reaching the fly was always around
562 1.1L/min. To create the gas dilutions for the odorants, four mass flow controllers (MFCs) were used
563 (Analyt-MTC) and controlled using a custom MATLAB (MathWorks) script and an Arduino board.
564 Another 3 MFCs were required to keep the constant airflows for the main airflow and the balancer
565 airflows. Odors were prepared in 20ml glass vials as a liquid volumetric dilution with a total volume of
566 5 mL in mineral oil. Airflow dilutions used are described in Table S3. Liquid dilutions were prepared
567 in 20 ml glass vials always to a total volume of 5 mL in mineral oil.
568
569 **Electrophysiology**
570 Single-sensillum recordings were performed as previously described[13] using a silver-chloride electrode
571 and glass pipettes filled with sensillum lymph ringer. Electrical signals were amplified using an
572 extracellular amplifier (EXT-02F-1, npi) with head stage (EXTEH), bandpass filtered (300–5000 Hz),
573 digitized at 20KHz using a NI board (NI-6212). Data were acquired with the MATLAB toolbox
574 kontroller[26] (https://github.com/emonetlab/kontroller). Spikes were sorted using a custom MATLAB
575 script. Odor delivery: flies were exposed to a constant airflow (1L/min) and an odor stimulus was
576 delivered by switching a 3-way solenoid valve that directed a secondary airflow (100 mL/min) through
577 a Pasteur pipette as in[13,38]. The pipette contained a filter paper with 50ml of the odor dilution. Volumetric

odor dilutions were prepared in either mineral oil or MiliQ Water. Stimuli were controlled by custom-made software in MATLAB and Arduino.

Pharmacology

Acetylcholine receptor blockage was performed using 100 µM atropine + 20 µM tubocurarine + 200 nM imidacloprid (IMI). Stock solutions of 2 mM atropine and 20 mM tubocurarine were prepared in water and aliquoted and frozen at -20ºC. Stock solution of 1 mM IMI was prepared in DMSO and kept at room temperature. Final solution was dissolved in saline solution used for *in vivo* calcium imaging and kept at 4 ºC.

GABA receptor blockage was done using 25 µM CGP54626 + 5 µM picrotoxin (PTX). Stock solutions of 25 mM CGP54626 and 100 mM PTX were prepared in DMSO, aliquoted and kept at -20ºC. Final solution was dissolved in saline solution used for *in vivo* calcium imaging and kept at 4 ºC.

For all pharmacology experiments, flies were prepared for *in vivo* calcium imaging as explained before, with the addition of a final step during dissection where the brain was de-sheathed. All flies were imaged before application of drug solutions with the same stimulation protocol used after drug was added in bath application.

For acetylcholine receptor blockage experiments, normal saline solution was replaced by 100 µM atropine + 20 µM tubocurarine + 200 nM IMI solution 2 consecutive times and then again 10 min after. Recordings were started 20 min after the drug solution was initially applied.

For GABA receptor blockage, normal saline solution was replaced by 25 µM CGP54626 + 5 µM PTX. This was repeated 1 min, 2 min and 10 min after this initial drug application. Recordings were started 40 min after the drug solution was initially applied.

Adaptation model: population response

We model the peak firing rate of a single ORNs, $F_{\mathrm{i}}(s)$, as a function of the odor stimulus, s, as

$$F_{\mathrm{i}}(s) = \alpha_i \left[\frac{\tanh(s - \beta_{\mathrm{i}}) + 1}{2} - \gamma_i \right] \qquad (1)$$

where we have included an explicit dependence on the parameters α_i, β_{i} and γ_i that control the amplitude-compression, sensitivity-shift, and amplitude-shift adaptation respectively. Neurons within the population are set with an initial random stimulus tuning β_{i} and the fixed parameters α_i and γ_i. The adapted firing rate, $F'_{\mathrm{peak}}(s)$, is described by the same equation but different parameters, $\beta'_{\mathrm{i}}, \alpha'_i$ and γ'_i, which are updated in a background response-dependent way. For the simulations in Fig. 1, we used the update rules,

$$I. \quad \beta'_{\mathrm{i}} = \beta_{\mathrm{i}} + c_\beta F_{\mathrm{i}}(s_B) \text{ fixed } \alpha_i, \gamma_i$$
$$II. \quad \alpha'_i = \alpha_i - c_\alpha F_{\mathrm{i}}(s_B) \text{ fixed } \beta_i, \gamma_i$$

$$III. \quad \gamma'_i = \gamma_i + c_\gamma F_{\mathrm{i}}(s_B) \text{ fixed } \alpha_i, \beta_i$$

with $c_\alpha = c_\gamma = 0.8$ and $c_\beta = 1$. We further tested that the specific values of these parameters do not affect our conclusions. For that we varied the parameters within the range $c_\alpha, c_\beta, c_\gamma \in [0.5, 1.5]$ and we computed the mean variance ratio between the first two principal components for increments of 0.1 in the parameters. For each adaptation mechanism we got the ratios $r_\alpha = 1.62 \pm 0.53, r_\beta = 15.46 \pm 0.76$ and $r_\gamma = 1.63 \pm 0.51$. Ratios near to unity indicate that both principal components contribute significantly to the population response, while large ratio values indicate a predominant representation of the first principal component. Altogether, we show that the results shown in Fig. 1 hold for different update rules of the parameters in Eq. (1).

Adaptation model: firing rate and calcium response

We model three different types of adaptation that we control throughout independent parameters α_i, β_i and γ_i of the response function in Eq. (1). As shown in the schematics of **Fig. 6a**, we consider that the postsynaptic calcium response of each ORN is a function of the difference between the ORN firing rate, $F_E(s)$, and an inhibitory rate, $F_I(s)$, coming from LNs, that is,

$$R_{Ca}[F(s,t)] = R[F_E(s,t) - F_I(s,t)], \tag{2}$$

where we consider $R[\cdot]$ to be a linear functional of the firing rate as suggested by **Fig. 2e**. We model the dynamics of each ORN firing rate as the exponential process,

$$F_E(s,t) = F(s)\left[exp\left(-\frac{t}{\tau_E}\right) + I_E\right] \tag{3}$$

where τ_E is the excitatory time constant, $F(s)$ is the firing rate described by Eq. (1) and I_E is the excitatory baseline. We consider the inhibitory rate to have the same dynamics and firing rate adaptation, inherited from the ORN responses, but different baseline $I_E - I_I = \Delta_I = 0.05$.

Using the excitatory and inhibitory functions described in Eq. (3), we find that the calcium response of Eq. (2) exhibits a smooth sustained response proportional to the difference between the excitatory and inhibitory rates, that is,

$$R_{ca}(s,t) = \Delta_I F(s).$$

The calcium sustained response to a given stimulus s in the presence of a background, s_B, is proportional to the sum of the sustained calcium response to the background and the stimulus calcium response after the firing rate is adapted, that is,

$$R'_{Ca}[F(s,s_B,t)] = R_{Ca}[F(s_B,t)] + R_{Ca}[F'(s,t)] \tag{4}$$

To achieve invariant calcium responses after adaptation, as observed in the experiments, we must ensure that Eq.(4) equals Eq.(1), meaning that the adapted firing rate to a given test stimulus s satisfies:

$$F'(s) = F(s) - F(s_B).$$

This implies that firing rate adaptation has to occur as a change in the response domain rather than in the stimulus domain. Using the functional form for firing rate defined in Eq. (1), we calculate the adaptation parameters that satisfy this condition for each type of adaptation strategy. Specifically, we calculate the adapted value of the parameters for the three adaptation mechanisms considered:

$$\begin{aligned} \beta' &= s - tanh^{-1}\left[2\left(\frac{F(s)-F(s_B)}{\alpha} + \gamma\right) - 1\right] && \text{for sensitivity-shift} \\ \alpha' &= \alpha\left[1 - \frac{F(s_B)}{F(s)}\right] && \text{for amplitude-compression} \\ \gamma' &= \gamma + \frac{F(s_B)}{\alpha} && \text{for amplitude-shift} \end{aligned} \tag{5}$$

This demonstrate that the only adaptation mechanism that depends uniquely on the background adaptation response and satisfies the calcium invariant condition is the amplitude-shift adaptation. The other two mechanisms require information of both the adapted and non-adapted responses, which are not accessible simultaneously to the circuit.

Adaptation model: effects of inter-glomerular activity

To understand how inter-glomerular activity further shapes the adapted responses of ORNs, we modeled a second inhibitory mechanism that reads out odor information from the population of ORNs, and acts at the single ORN level (see Fig. 8). Specifically, we introduce in our model an LN neuron that connects to several glomeruli[31,32] and provides an inhibitory input to the presynaptic terminals. This can be formalized by modifying Eq. (1) as,

$$R_{Ca}[F(s,t)] = R[F_E(s,t) - F_I(s,t) - F_G(s,t)], \qquad (6)$$

where $F_G(s,t) = \sum_i \omega_i F_i(s,t)$ corresponds to the LN term that integrates the ORN population activity. Assuming that the dynamics of the global feedback is slower than the dynamics of the local feedback, our previous arguments hold up to Eq (4). Similarly as we did before, we use Eq. (6) to write a new relation between the calcium responses of non-adapted and adapted ORNs:

$$F'(s) = F(s) - F(s_B) - F_G(s) + F_G(s_B) + F'_G(s). \qquad (7)$$

We showed in **Fig. 1** that a population of ORNs encodes both stimulus intensity and contrast in a two-dimensional manifold, making it possible for two downstream neurons to extract such an information as a linear combination of single ORNs. Consequently, we assume that the LN neuron that connects to multiple glomeruli extracts contrast information from the population such that $F_G(s,t) = s - s_B$, which at zero background equals the stimulus intensity. We can then write Eq. (7) as,

$$F'(s) = F(s) - F(s_B) - s + s_B + s - s_B, \qquad (8)$$

showing that the amplitude-shift mechanism continues to support ON-background invariance if contrast information is extracted from ORN populations by inter-glomerular LNs. In the absence of an odor background, the encoding of contrast information equals the encoding of the intensity value, which is in agreement with the literature on the role of inhibitory LNs[31,32,56].

Acknowledgment

We thank Filippo Calzolari for reading the first version of the manuscript, Giovanni D'Uva for developing methodology, Christopher Schnaitmann for help with *in vivo* imaging and comments on the manuscript, members of the Martelli and Silies lab for discussions, Sabine Schmitt, Simone Renner and Jonas Chojetzki for technical and administrative support. We thank Mathias Böhme for help in the planning of the mutagenesis of the Unc13 C1 domain.

Funding

This work was supported by the DFG grant MA7804/2-1 to CM, the Research Unit FOR5289 (project P5 to MA and P6 to CM), the Emmy Noether Programme (project 261020751) and the Novo Nordisk Foundation (Young Investigator Award NNF19OC0056047) to AMW.

Author contribution

Conceptualization: SCB, CM
Methodology: SCB, LR, AMW, MS, CM
Investigation: SCB, LR, CM
Formal analysis: LR, CM
Visualization: SCB, LR, CM
Supervision: CM
Writing—original draft: LR, CM
Writing—review & editing: SCB, LR, AMW, MS, CM

References

1. Wark, B., Lundstrom, B. & Fairhall, A. Sensory adaptation. *Curr Opin Neurobiol* **17**, 423–429 (2007).
2. Laughlin, S. B. The role of sensory adaptation in the retina. *Journal of Experimental Biology* **146**, 39–62 (1989).
3. Simoncelli, E. P. Vision and the statistics of the visual environment. *Curr Opin Neurobiol* **13**, 144–149 (2003).
4. Brenner, N., Bialek, W. & De Ruyter Van Steveninck, R. Adaptive Rescaling Maximizes Information Transmission. *Neuron* **26**, 695–702 (2000).
5. Laughlin, S. B. & Hardie, R. C. Common strategies for light adaptation in the peripheral visual systems of fly and dragonfly. *Journal of Comparative Physiology □ A* **128**, 319–340 (1978).
6. Malnic, B., Hirono, J., Sato, T. & Buck, L. B. Combinatorial receptor codes for odors. *Cell* (1999) doi:10.1016/S0092-8674(00)80581-4.
7. Hallem, E. a & Carlson, J. R. Coding of odors by a receptor repertoire. *Cell* **125**, 143–60 (2006).
8. Benda, J. Neural adaptation. *Current Biology* **31**, R110–R116 (2021).
9. Weber, A. I., Krishnamurthy, K. & Fairhall, A. L. Coding Principles in Adaptation. *Annu Rev Vis Sci* **5**, 427–449 (2019).
10. Gutnisky, D. A. & Dragoi, V. Adaptive coding of visual information in neural populations. *Nature 2008 452:7184* **452**, 220–224 (2008).
11. Reisert, J. & Matthews, H. R. Adaptation of the odour-induced response in frog olfactory receptor cells. *Journal of Physiology* (1999) doi:10.1111/j.1469-7793.1999.0801n.x.
12. Nagel, K. I. & Wilson, R. I. Biophysical mechanisms underlying olfactory receptor neuron dynamics. *Nat Neurosci* **14**, 208–216 (2011).
13. Martelli, C., Carlson, J. R. & Emonet, T. Intensity invariant dynamics and odor-specific latencies in olfactory receptor neuron response. *Journal of Neuroscience* **33**, (2013).
14. Strausfeld, C. Z. & Kaissling, K.-E. Localized adaptation processes in olfactory sensilla of Saturniid moths. *Chem Senses* **11**, 499–512 (1986).
15. Lemon, W. & Getz, W. Temporal resolution of general odor pulses by olfactory sensory neurons in American cockroaches. *Journal of Experimental Biology* **200**, 1809–1819 (1997).
16. Raman, B., Joseph, J., Tang, J. & Stopfer, M. Temporally diverse firing patterns in olfactory receptor neurons underlie spatiotemporal neural codes for odors. *Journal of Neuroscience* **30**, 1994–2006 (2010).
17. Kurahashi, T. & Menini, A. Mechanism of odorant adaptation in the olfactory receptor cell. *Nature* **385**, 725–729 (1997).
18. Dalton, P. Psychophysical and behavioral characteristics of olfactory adaptation. *Chem Senses* **25**, 487–492 (2000).
19. Ramaswami, M. Network plasticity in adaptive filtering and behavioral habituation. *Neuron* **82**, 1216–1229 (2014).
20. Sinding, C. *et al.* New determinants of olfactory habituation. *Sci Rep* **7**, 41047 (2017).
21. Wilson, D. A. Habituation of odor responses in the rat anterior piriform cortex. *J Neurophysiol* **79**, 1425–1440 (1998).
22. Fishilevich, E. *et al.* Chemotaxis behavior mediated by single larval olfactory neurons in Drosophila. *Current Biology* (2005) doi:10.1016/j.cub.2005.11.016.
23. Baker, K. L. *et al.* Algorithms for Olfactory Search across Species. *J. Neurosci.* **38**, 9383–9389 (2018).
24. Sourjik, V. & Wingreen, N. S. Responding to chemical gradients: bacterial chemotaxis. *Curr Opin Cell Biol* **24**, 262–268 (2012).
25. Louis, M. Mini-brain computations converting dynamic olfactory inputs into orientation behavior. *Curr Opin Neurobiol* **64**, 1–9 (2020).
26. Gorur-Shandilya, S., Demir, M., Long, J., Clark, D. A. & Emonet, T. Olfactory receptor neurons use gain control and complementary kinetics to encode intermittent odorant stimuli. *Elife* **6**, e27670 (2017).

27. Martelli, C. & Storace, D. A. Stimulus Driven Functional Transformations in the Early Olfactory System. *Front Cell Neurosci* **15**, (2021).
28. Brandão, S. C., Silies, M. & Martelli, C. Adaptive temporal processing of odor stimuli. *Cell Tissue Res* **383**, 125–141 (2021).
29. Su, C.-Y., Menuz, K. & Carlson, J. R. Olfactory Perception: Receptors, Cells, and Circuits. *Cell* **139**, 45–59 (2009).
30. Kazama, H. & Wilson, R. I. Homeostatic matching and nonlinear amplification at identified central synapses. *Neuron* **58**, 401–413 (2008).
31. Olsen, S. R. & Wilson, R. I. Lateral presynaptic inhibition mediates gain control in an olfactory circuit. *Nature* **452**, 956–960 (2008).
32. Olsen, S. R., Bhandawat, V. & Wilson, R. I. Divisive normalization in olfactory population codes. *Neuron* **66**, 287–299 (2010).
33. Banerjee, A. *et al.* An Interglomerular Circuit Gates Glomerular Output and Implements Gain Control in the Mouse Olfactory Bulb. *Neuron* **87**, 193–207 (2015).
34. Laughlin, S. B. & Hardie, R. C. Common strategies for light adaptation in the peripheral visual systems of fly and dragonfly. *Journal of Comparative Physiology □ A* (1978) doi:10.1007/BF00657606.
35. Bates, A. S. *et al.* Complete Connectomic Reconstruction of Olfactory Projection Neurons in the Fly Brain. *Current Biology* **30**, 3183-3199.e6 (2020).
36. Strutz, A. *et al.* Decoding odor quality and intensity in the Drosophila brain. *Elife* **3**, e04147 (2014).
37. Liang, L. *et al.* GABAergic Projection Neurons Route Selective Olfactory Inputs to Specific Higher-Order Neurons. *Neuron* **79**, 917–931 (2013).
38. Martelli, C. & Fiala, A. Slow presynaptic mechanisms that mediate adaptation in the olfactory pathway of Drosophila. *Elife* **8**, (2019).
39. Cafaro, J. Multiple sites of adaptation lead to contrast encoding in the Drosophilaolfactory system. *Physiol Rep* **4**, e12762 (2016).
40. Chamberland, S. *et al.* Fast two-photon imaging of subcellular voltage dynamics in neuronal tissue with genetically encoded indicators. *Elife* **6**, (2017).
41. Barth-Maron, A., D'Alessandro, I. & Wilson, R. I. Interactions between specialized gain control mechanisms in olfactory processing. *Curr Biol* **33**, 5109-5120.e7 (2023).
42. Jusyte, M. *et al.* Unc13A dynamically stabilizes vesicle priming at synaptic release sites for short-term facilitation and homeostatic potentiation. *Cell Rep* **42**, (2023).
43. Augustin, I., Rosenmund, C., Südhof, T. C. & Brose, N. Munc13-1 is essential for fusion competence of glutamatergic synaptic vesicles. *Nature* **400**, 457–461 (1999).
44. Walter, A. M., Böhme, M. A. & Sigrist, S. J. Vesicle release site organization at synaptic active zones. *Neurosci Res* **127**, 3–13 (2018).
45. Varoqueaux, F. *et al.* Total arrest of spontaneous and evoked synaptic transmission but normal synaptogenesis in the absence of Munc13-mediated vesicle priming. *Proc Natl Acad Sci U S A* **99**, 9037–9042 (2002).
46. Richmond, J. E., Davis, W. S. & Jorgensen, E. M. UNC-13 is required for synaptic vesicle fusion in C. elegans. *Nat Neurosci* **2**, 959–964 (1999).
47. Böhme, M. A. *et al.* Rapid active zone remodeling consolidates presynaptic potentiation. *Nat Commun* **10**, (2019).
48. Böhme, M. A. *et al.* Active zone scaffolds differentially accumulate Unc13 isoforms to tune Ca(2+) channel-vesicle coupling. *Nat Neurosci* **19**, 1311–1320 (2016).
49. Fulterer, A. *et al.* Active Zone Scaffold Protein Ratios Tune Functional Diversity across Brain Synapses. *Cell Rep* **23**, 1259–1274 (2018).
50. Dittman, J. S. Unc13: a multifunctional synaptic marvel. *Curr Opin Neurobiol* **57**, 17–25 (2019).
51. Michelassi, F., Liu, H., Hu, Z. & Dittman, J. S. A C1-C2 Module in Munc13 Inhibits Calcium-Dependent Neurotransmitter Release. *Neuron* **95**, 577-590.e5 (2017).
52. Taschenberger, H., Woehler, A. & Neher, E. Superpriming of synaptic vesicles as a common basis for intersynapse variability and modulation of synaptic strength. *Proc Natl Acad Sci U S A* **113**, E4548–E4557 (2016).

53. Rhee, J. S. *et al.* β phorbol ester- and diacylglycerol-induced augmentation of transmitter release is mediated by Munc13s and not by PKCs. *Cell* **108**, 121–133 (2002).
54. Betz, A. *et al.* Munc13-1 is a presynaptic phorbol ester receptor that enhances neurotransmitter release. *Neuron* **21**, 123–136 (1998).
55. Basu, J., Betz, A., Brose, N. & Rosenmund, C. Munc13-1 C1 domain activation lowers the energy barrier for synaptic vesicle fusion. *J Neurosci* **27**, 1200–1210 (2007).
56. Root, C. M. *et al.* A presynaptic gain control mechanism fine-tunes olfactory behavior. *Neuron* **59**, 311–321 (2008).
57. Ganguli, D. & Simoncelli, E. P. Efficient sensory encoding and Bayesian inference with heterogeneous neural populations. *Neural Comput* **26**, 2103–2134 (2014).
58. Keller, A. & Vosshall, L. B. Influence of odorant receptor repertoire on odor perception in humans and fruit flies. *Proc Natl Acad Sci U S A* **104**, 5614–5619 (2007).
59. Zwicker, D., Murugan, A. & Brenner, M. P. Receptor arrays optimized for natural odor statistics. *Proc Natl Acad Sci U S A* **113**, 5570–5575 (2016).
60. Tesileanu, T., Cocco, S., Monasson, R. & Balasubramanian, V. Adaptation of olfactory receptor abundances for efficient coding. *Elife* **8**, (2019).
61. Cognigni, P., Felsenberg, J. & Waddell, S. Do the right thing: neural network mechanisms of memory formation, expression and update in Drosophila. *Curr Opin Neurobiol* **49**, 51–58 (2017).
62. Ling, D., Zhang, L., Saha, D., Chen, A. B. & Raman, B. Adaptation invariant concentration discrimination in an insect olfactory system. *Elife* **12**, (2023).
63. Gomez-Marin, A., Stephens, G. J. & Louis, M. Active sampling and decision making in Drosophila chemotaxis. *Nature Communications 2011 2:1* **2**, 1–10 (2011).
64. Gepner, R., Skanata, M. M., Bernat, N. M., Kaplow, M. & Gershow, M. Computations underlying Drosophila photo- taxis, odor-taxis, and multi-sensory integration. *Elife* **4**, (2015).
65. Vickers, N. J. Mechanisms of animal navigation in odor plumes. *https://doi.org/10.2307/1542524* **198**, 203–212 (2000).
66. Murlis, J., Elkinton, J. S. & Cardé, R. T. Odor plumes and how insects use them. *Annu Rev Entomol* **37**, 505–532 (1992).
67. Kadakia, N. *et al.* Odour motion sensing enhances navigation of complex plumes. *Nature 2022 611:7937* **611**, 754–761 (2022).
68. Dolan, M. J. *et al.* Neurogenetic dissection of the drosophila lateral horn reveals major outputs, diverse behavioural functions, and interactions with the mushroom body. *Elife* **8**, (2019).
69. Frechter, S. *et al.* Functional and anatomical specificity in a higher olfactory centre. *Elife* (2019) doi:10.7554/eLife.44590.
70. Taisz, I. *et al.* Generating parallel representations of position and identity in the olfactory system. *Cell* **186**, 2556-2573.e22 (2023).
71. Kim, H. S. & Jeanne, J. M. Divergent short-term plasticity creates parallel pathways for computation and behavior in an olfactory circuit. doi:10.1101/2024.04.29.591740.
72. Álvarez-Salvado, E. *et al.* Elementary sensory-motor transformations underlying olfactory navigation in walking fruit-flies. *Elife* **7**, e37815 (2018).
73. Murmu, M. S., Stinnakre, J. & Martin, J. R. Presynaptic Ca2+ stores contribute to odor-induced responses in Drosophila olfactory receptor neurons. *Journal of Experimental Biology* (2010) doi:10.1242/jeb.046474.
74. Murmu, M. S., Stinnakre, J., Réal, E. & Martin, J. R. Calcium-stores mediate adaptation in axon terminals of Olfactory Receptor Neurons in Drosophila. *BMC Neurosci* (2011) doi:10.1186/1471-2202-12-105.
75. Silva, M., Tran, V. & Marty, A. Calcium-dependent docking of synaptic vesicles. *Trends Neurosci* **44**, 579–592 (2021).
76. Wang, X., Roberts, P. A., Yoshimatsu, T., Lagnado, L. & Baden, T. Amacrine cells differentially balance zebrafish color circuits in the central and peripheral retina. *Cell Rep* **42**, 112055 (2023).
77. Brand, P. *et al.* The origin of the odorant receptor gene family in insects. *Elife* **7**, (2018).
78. Ruta, V. *et al.* A dimorphic pheromone circuit in Drosophila from sensory input to descending output. *Nature* **468**, 686–690 (2010).

79. Stensmyr, M. C. *et al.* A conserved dedicated olfactory circuit for detecting harmful microbes in drosophila. *Cell* **151**, 1345–1357 (2012).
80. Kondo, S. & Ueda, R. Highly improved gene targeting by germline-specific Cas9 expression in Drosophila. *Genetics* **195**, 715–721 (2013).

Supplementary Material

Table S1: Key resources

Reagent or Resource	Source	Identifier
Chemicals		
Methyl acetate	Sigma-Aldrich Co	Art. #45999, CAS 79-20-9
2-butanone	Carl Roth	Art. #T920.1, CAS 78-93-3
Mineral Oil	Sigma-Aldrich Co	Art. #330779, CAS 8042-47-5
CGP 54626 hydrochloride	Tocris Bioscience	Art. #1088, CAS 149184-21-4
Picrotoxin	Sigma-Aldrich Co	Art. #P1675, CAS 124-87-8
Atropine	Sigma-Aldrich Co	Art. #A0132, CAS 51-55-8
Tubocurarine	Sigma-Aldrich Co	Art. #T2379, CAS 6989-98-6
Imidacloprid	Sigma-Aldrich Co	Art. #37894, CAS 138261-41-3
All trans retinal	Sigma-Aldrich Co	Art. #R2500, CAS 116-31-4
Bondic cartridge with Bondic liquid plastic	Bondic	Art. #BONKART
Bondic UV-LED	Bondic	Art. #BONLED
Experimental Models: Organisms/Strains		
D. melanogaster: or42b-Gal4	Bloomington Drosophila Stock Center (BDSC)	RRID: BDSC_9972
D. melanogaster: or10a-Gal4	BDSC	RRID: BSDC_9944
D. melanogaster: GH146-Gal4	Gift from A. Fiala	Gift from A. Fiala
D. melanogaster: orco-Gal4	BDSC	RRID: BSDC_23292
D. melanogaster: UAS-GCaMP6f	BDSC	RRID: BSDC_42747
D. melanogaster: UAS-CsChrimson	BDSC	RRID: BSDC_82180
D. melanogaster: UAS- shibire^{ts}	Gift from M. Silies	
D. melanogaster: Unc13H1723K	Gift from A. Walter	
D. melanogaster: UAS-ASAP2s	Gift from T. Clandinin	
Software and algorithms		
Fiji		RRID: SCR_002285
MATLAB	MathWorks	RRID: SCR_001622
Adobe Illustrator	Adobe	RRID: SCR_010279

887 **Table S2: Genetic *D. melanogaster* strains**
888

Name	Genotype	Figure
GH146 > GCaMP6f	w+; UAS-GCaMP6f/GH146-Gal4 ; +	3
GH146 > ASAP2s		3
Or42b > GCaMP6f, csChrimson	w+; UAS-GCaMP6f/+; or42b-Gal4/UAS-csChrimson	4
Or42b > GCaMP6f, shibire^{ts}	w+; UAS-GCaMP6f/+; or42b-Gal4/UAS-shibire^{ts}	5
orco > GCaMP6f	w+; UAS-GCaMP6f/+; orco-GAL4/+	5
orco > GCaMP6f; Unc13H1723K	w+; UAS-GCaMP6f/+; orco-GAL4/+; Unc13H1723K	7
GH146 > GCaMP6f	w+; UAS-GCaMP6f/GH146-Gal4 ; +	7
GH146 > GCaMP6f; Unc13H1723K	w+; UAS-GCaMP6f/GH146-Gal4 ; +; Unc13H1723K	7

889
890
891
892
893
894 **Table S3: Airflow dilutions for odor**
895

	Odor airflow (sccm)	Equivalent dilution
C4	0.03	$10^{-4.5}$
C5	0.10	10^{-4}
C6	0.30	$10^{-3.5}$
C7	1	10^{-3}
C8	3	$10^{-2.5}$
C9	10	10^{-2}

896

Supplementary Figures

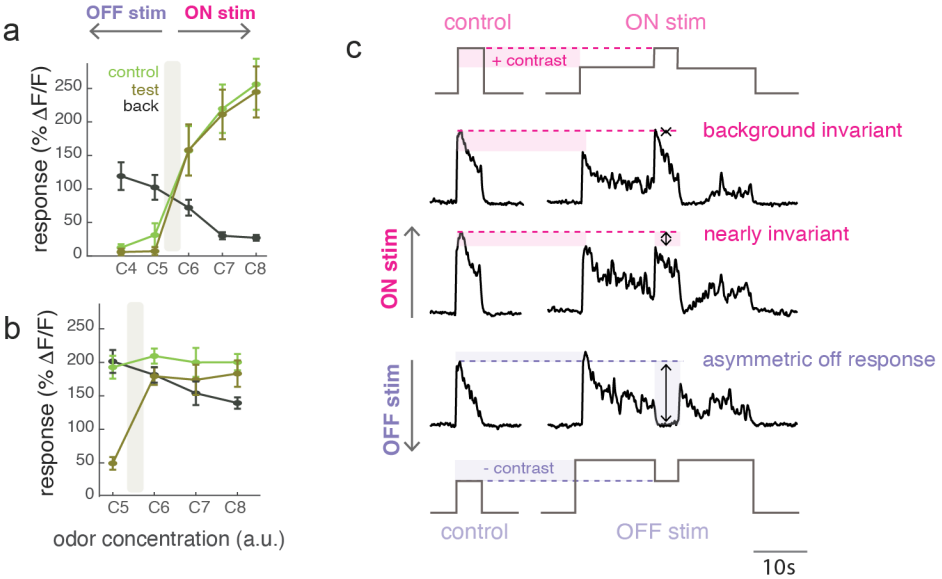

Figure S1: PNs response to ON and OFF stimuli. To cover a range of ON and OFF responses of PNs, we conducted two sets of experiments using different liquid solutions of the odors. To generate main **Fig. 3** we analyzed the single trials of these two datasets. Here we show mean responses (**a, b**) and some examples of response to small contrast stimuli (**c**).

a-b) Peak calcium response to different combinations of ON, OFF and background stimuli using methyl acetate. *Green*: mean response to non-adapted control. *Black*: mean response to background stimulus. *Dark green*: mean response to the same stimulus as in green after 15 seconds of background adaptation. Error bars indicate sem, the shaded area indicated the stimulus that equals the background concentration. Liquid dilution of methyl acetate for the background was 10^{-4} in **a)** and 10^{-3} in **b)**, therefore the higher background response in **b)**. The liquid dilution for the pulse was 10^{-2} in **a)** and 10^{-3} in **b)**. Labels on the x-axis corresponds to gas phase dilutions generated by the odor delivery system as indicated in **table S3**. **c)** Three single trials from the dataset showing responses to ON and OFF stimuli with small contrast. The shaded area indicates the difference in response between test and background stimulus. The dotted line indicates the response to the control stimulus. These traces show how a small positive contrast leads to nearly perfectly invariant response (same as controls), while a small negative contrast leads to a strong decrease in calcium, much lower than the test stimulus amplitude.

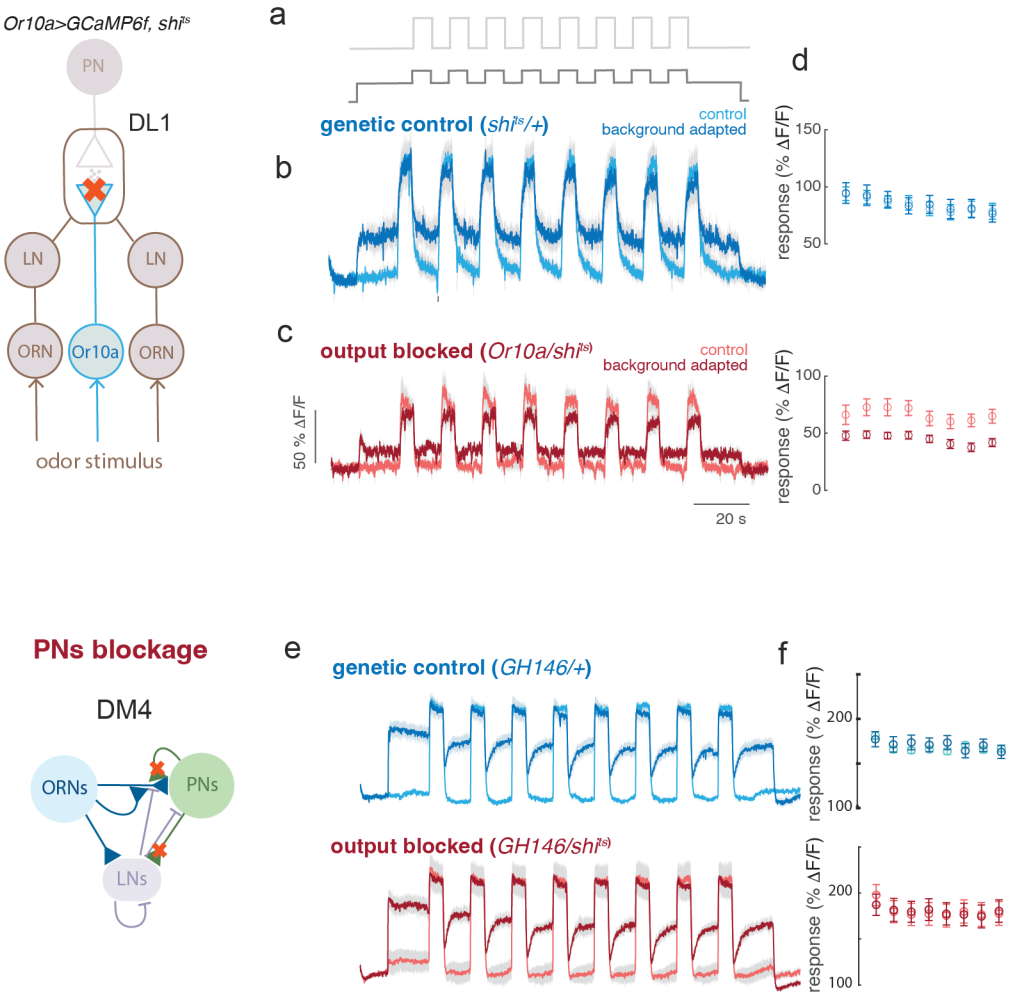

Figure S2: Role of synaptic release for ORN background invariance.
a) Genetic blockage of Or10a-ORNs neurotransmitter release. Stimulation protocol in control (light gray) and background adapted conditions (dark gray). **b)** Calcium response of the DL1 glomerulus in genetic control flies showing background-invariant responses. **c)** Calcium response in flies with blocked ORN synapses showing background dependent responses. **d)** Quantification of peak response for each of the 8 test pulses. Error bars indicate sem (N=4, 7). **e)** Blocking of PN synaptic output does not affect ORN presynaptic calcium responses. Traces represent mean calcium responses of DM4 ORNs in control (light colors) and background adapted conditions (dark colors) for control (blue) and test flies (red). Test flies express shi^{ts} under control of GH146-GAL4 that labels PNs. **f)** Quantification of peak response for each of the 8 test pulses. Error bars indicate sem.

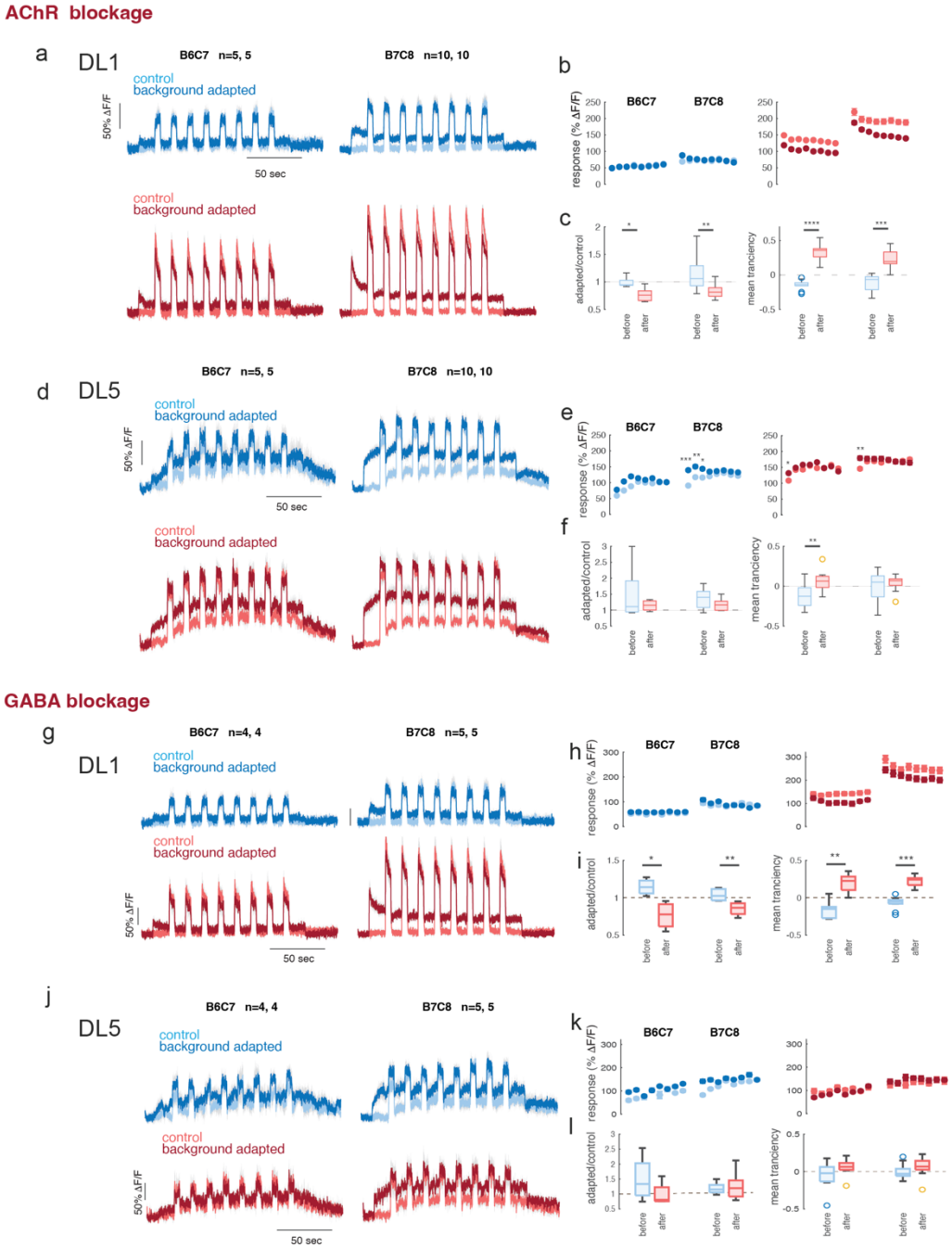

Figure S3: Glomerulus specific mechanisms for presynaptic calcium modulation.
a) Pharmacological blockage of Ach-R. Traces represent mean calcium responses of DL1 ORNs in control (light colors) and background adapted conditions (dark colors) before (blue) and after (red) drug application (100 µM atropine + 20 µM tubocurarine + 200 nM imi, see Methods). **b)** Quantification of peak response for each of the 8 test pulses. Error bars indicate sem but might not be visible.**c)** Boxplot quantification of the degree of adaptation and response transiency, indicating median, quartiles max/min and outliers. **d-e-f)** same as **a-b-c)** for glomerulus DL5. **g)** Pharmacological blockage of GABA-R. Traces represent mean calcium responses of DL1 ORNs in control (light colors) and background adapted conditions (dark colors) before (blue) and after (red) drug application (25 µM CGP54626 + 5 µM picrotoxin, see Methods). **h-i)** same quantification as in **b-c). j-k-l)** same as **g-h-i)** for glomerulus DL5. *p<0.05, **p<0.01, ***p<0.001, sample size is indicated for each dataset in the figure.

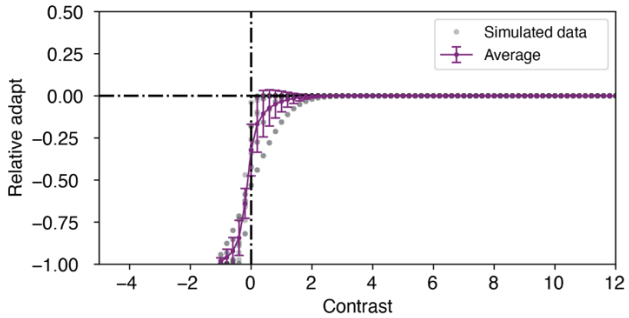

Figure S4: Modeling PNs relative adaptation for different contrast stimuli. We model the responses of PN neurons in a background adapted condition as a noisy process with probability $\mathrm{N}(s - s_B, \sigma)$, where s_B is the background stimulus and σ is the noise std. We simulate PN responses across different contrast stimuli and show that a standard deviation of $\sigma = 0.5$ fits the experimental observations shown in **Fig. 3c**. For each contrast value, we average the relative adaptation over a set of 10 different background conditions ranging from -4 to 4 in the stimulus log. scale.